Supporting information

Bronze TiO_2 photocatalysis facilitates solution plasma production of H_2O_2

Yanhui Li, Changhua Wang [*] , Qi Wu, Yuanyuan Li, Shuang Liang, Dexin Jin, He Ma, Xintong Zhang[*]

Key Laboratory of UV-Emitting Materials and Technology of Chinese Ministry of Education, Northeast Normal University, 5268 Renmin Street, Changchun 130024, P.R. China

[*] Corresponding authors: wangch100@nenu.edu.cn; xtzhang@nenu.edu.cn

1. Experiment

1.1 Chemicals

All solvents and chemicals used without further purification. Titanium dioxide (Degussa, P25); Sodium chloride (NaCl, AR, 99%); Anhydrous sodium carbonate (Na_2CO_3, AR, 99.8%); Disodium phosphate dodecahydrate ($Na_2HPO_4 \cdot 12H_2O$，GR, 99%); Sulfuric acid (H_2SO_4, AR, 99%).

1.2 Other TiO_2 samples

Anatase TiO_2, purchased from Aladdin, with a particle size of less than or equal to 400 nm and a purity greater than 99.5%. Rutile TiO_2, also from Aladdin, with a particle size of 100-300 nm and a purity greater than 99.8%. Commercial P25 was acquired from Degussa. Other TiO_2(B) samples were synthesized according to literature methods, specifically TiO_2(B) Ref-1 referenced from Chem. Comm., 2010, 46, 6801, and TiO_2(B) Ref-2 referenced from Dalton Trans., 2015, 44, 13331.

1.3 Scheme for synthesis of bronze TiO_2

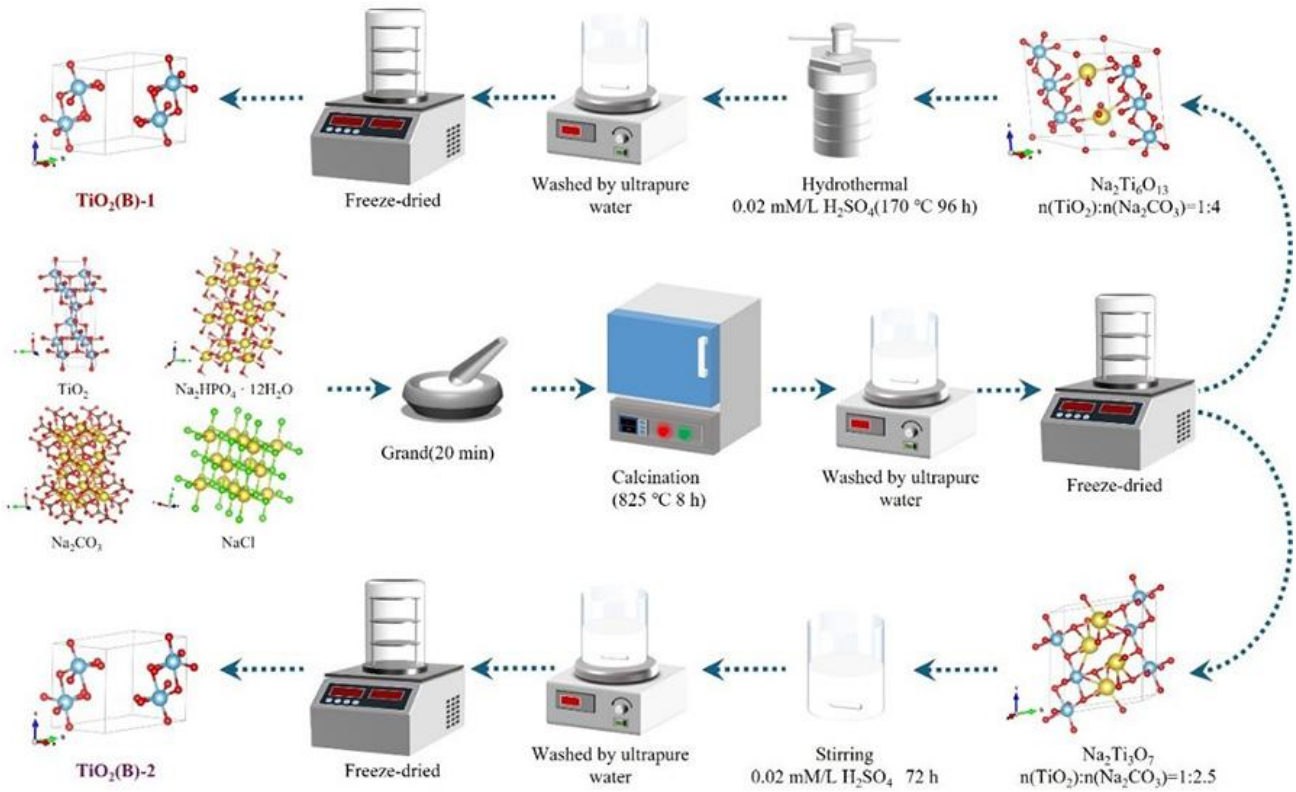

Figure S1. Scheme for preparation of bronze TiO_2 by different routes.

1.4 Materials characterization

The crystal structure and phase were characterized with X-ray diffraction (XRD, Rigaku D/max-2500, X-ray diffractometer), using Cu Kα radiation (λ = 1.5406 A) at 40 kV and 40 mA with a scan rate of 20°/min. Raman spectra were recorded on the Horiba Raman spectrometer, with a Sapphire semiconductor laser source of 488 nm wavelength. The surface morphology of the samples were recorded with a FEI Quanta-250 field-emission scanning electron microscope (SEM). Transmission electron micrographs (TEM) and high-resolution transmission electron micrographs (HRTEM) of the samples were recorded with a JEOL JEM-2100 transmission electron microscope at an acceleration voltage of 200 kV. UV-Vis diffuse reflectance (DR) spectra were recorded on a JASCO V700 UV-Vis-NIR spectrophotometer, using $BaSO_4$ as reference. The metal elements of the samples were quantified with a PE Avio 200 Plasma spectrometer (ICP-OES).

1.5 Measurement of H_2O_2

In this study, we calculate the content of H_2O_2 by UV spectroscopic calibration method. Three

solutions were configured in advance, solution A: 0.1 g of N,N-diethyl-p-phenylenediamine (DPD) was dissolved in 10 ml of sulfuric acid solution(0.05 M); solution B: 0.01 g of peroxidase (POD) was dissolved in 10 ml of secondary ionized water; solution C: Na_2HPO_4 solution and NaH_2PO_4 solution both of 0.1 mol/L. Test procedure for H_2O_2 content was as follows: 100 μL of the solution to be tested was taken, 6 mL of solution C (phosphate buffer) was added, and then 100 μL of solution A and B were added in turn, and the liquid to be tested showed red color after mixed well. Then measure absorbance of the solution using a Shimadzu UV-2600 spectrophotometer (range from 190 to 900 nm), and absorbance value at 552 nm was counted and substituted into the calibration curve to calculate concentration of H_2O_2. The calibration curve was calculated as Y = 0.000387987 x - 0.04839 with a coefficient of determination $R^2 = 0.99$. Where Y is the peak of spectral line at 552 nm and x is the concentration of solution to be measured.

1.6 The density functional theory (DFT) calculation:

a. Selection and Optimization of TiO_2 Structure

Considering computational resources, we selected the (101) surface of anatase TiO_2 and the (001) surface of bronze TiO_2, constructing six-layer unit cells with a 15 Å vacuum layer, which were then optimized using the Perdew-Burke-Ernzerhof (PBE) functional in VASP. The electronic exchange-correlation interactions were described by the PBE functional within the generalized gradient approximation (GGA). The electron-ion interactions were treated with the projector augmented-wave (PAW) pseudopotentials. The convergence criterion for total energy was set to 10^{-5} eV, and the force convergence criterion for each atom was set to 0.02 eV/Å. Brillouin zone sampling was performed using a 3×3×1 k-point mesh.

b. Ab initio molecular dynamics (AIMD) simulations.

To determine the structural stability of H_2O_2 molecules on different crystalline phases of TiO_2, we conducted AIMD simulations. All AIMD calculations are carried out in the CP2K 2024 package. The Gaussian and plane-wave methods in the Quickstep module were employed to calculate the energies and forces. Subsequently, 26 H_2O_2 molecules were introduced into the vacuum layer. By fixing the bottom layer of TiO_2, the thermodynamic stabilization model was obtained through AIMD kinetic simulations at a constant temperature for 20 ps based on GFX1-xtb, utilizing a V-rescale thermostat at 300 K and 1 bar during the simulations. The k-point sampling is limited to the Γ point only.

c. Radial Distribution Function (RDF) calculation

RDF is used to describe the distribution of particles relative to a reference particle at a given distance *r*. It reflects how particle density varies with distance and is commonly used to analyze the microstructure of materials and the interactions between particles. The value of the RDF, *g*(*r*), indicates the probability density of finding other particles at a distance r from the reference particle.

The mathematical expression of RDF is: $g(r) = \frac{N(r)}{\rho V}$

$N(r)$: The average number of particles within the shell width dr at a distance of r from the reference particle; ρ: The average particle density of the system; V: The volume of the box.

2. Other Figures and Tables

Table S1. ICP determination of sodium content in different samples

Catalysts	Sodium(mg/kg)	Proton exchange rate(%)
$Na_2Ti_6O_{13}$	86947.69	/
TiO_2(B)-1	982.61	98.87
$Na_2Ti_3O_7$	97202.49	/
TiO_2(B)-2	29393.69	69.76

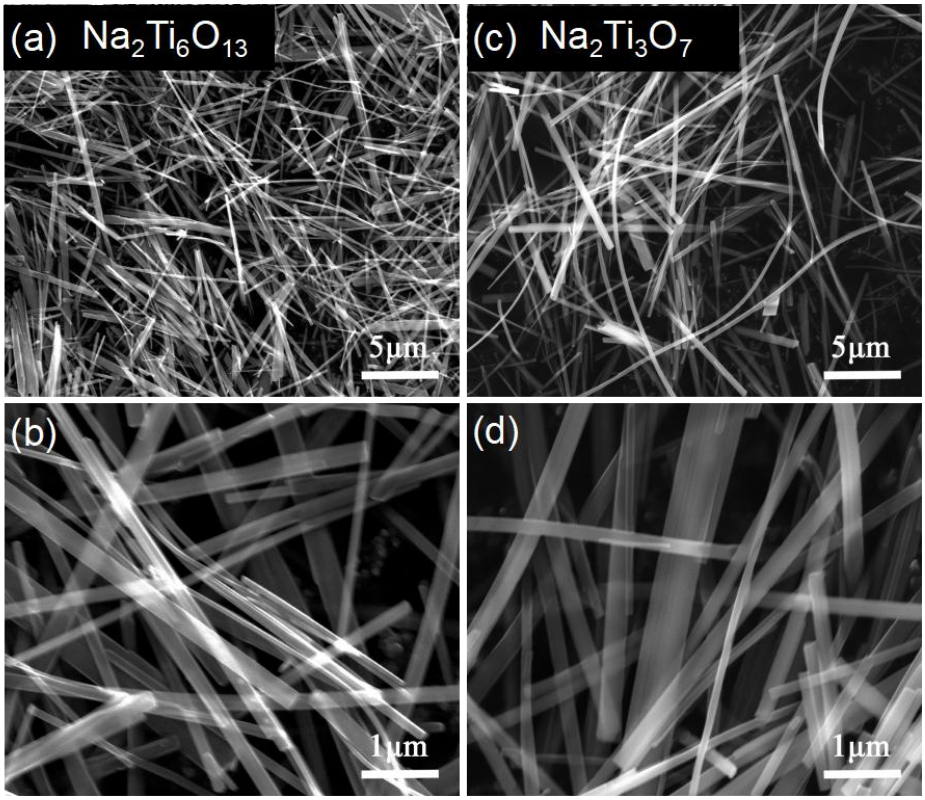

Figure S2. SEM images of different samples: (a, b) $Na_2Ti_6O_{13}$ nanobelts; (c, d) $Na_2Ti_3O_7$ nanobelts.

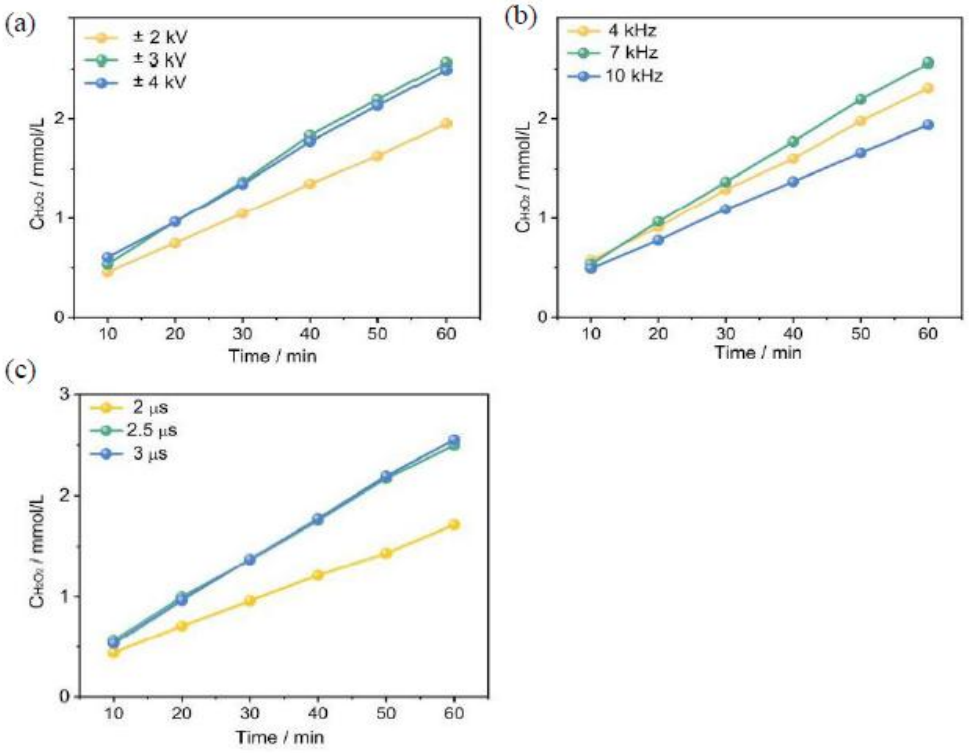

Figure S3. Effects of plasma parameters on the production of H_2O_2: (a) voltage; (b) frequency; (c) pulse width

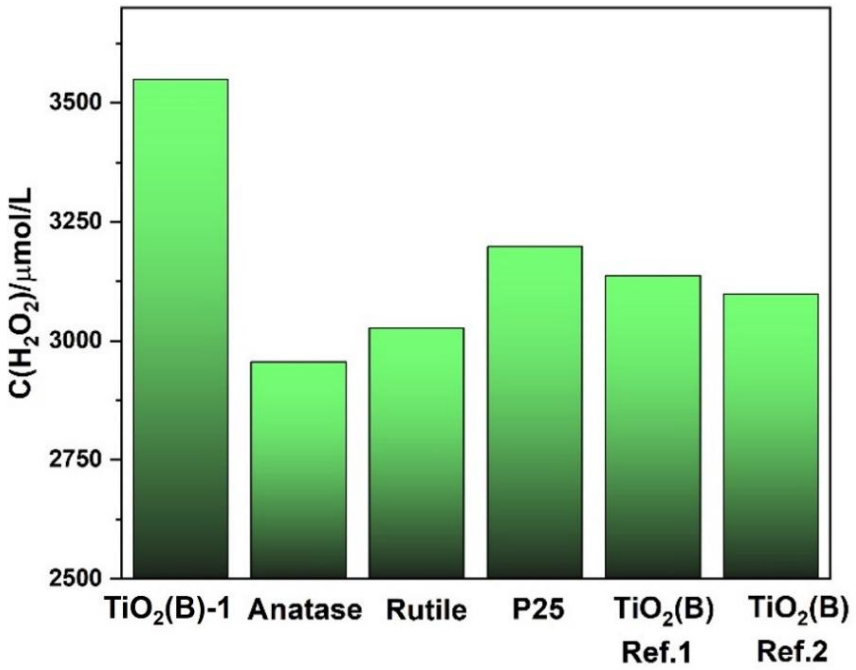

Figure S4. Comparison of activity over different TiO_2 samples in plasma catalysis. (Ref. 1: Chem. Comm., 2010, 46, 6801; Ref.2: Dalton Trans.,2015, 44, 13331.)

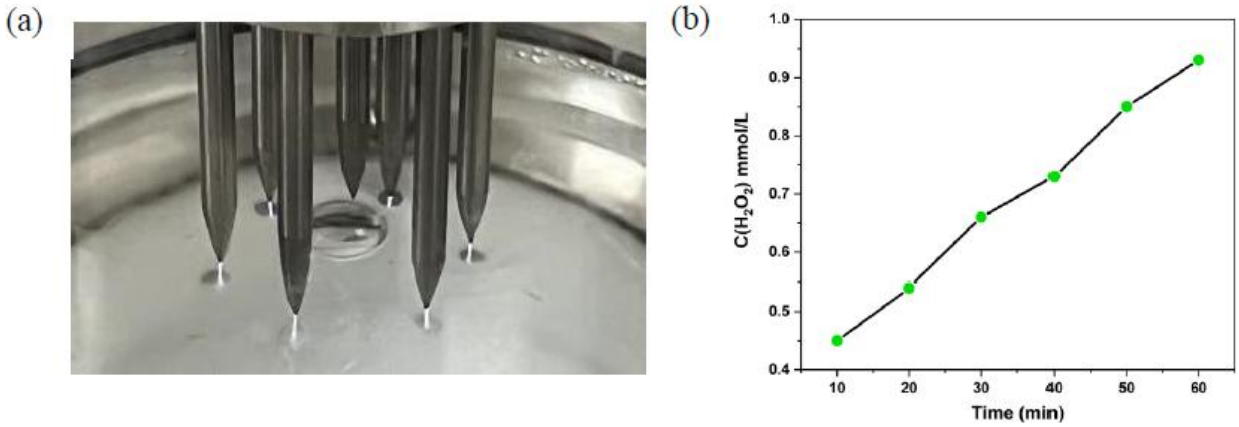

Figure S5. (a) Photograph of gas phase plasma for H_2O_2 production; (b) Production of H_2O_2 via plasma discharge in gas phase.

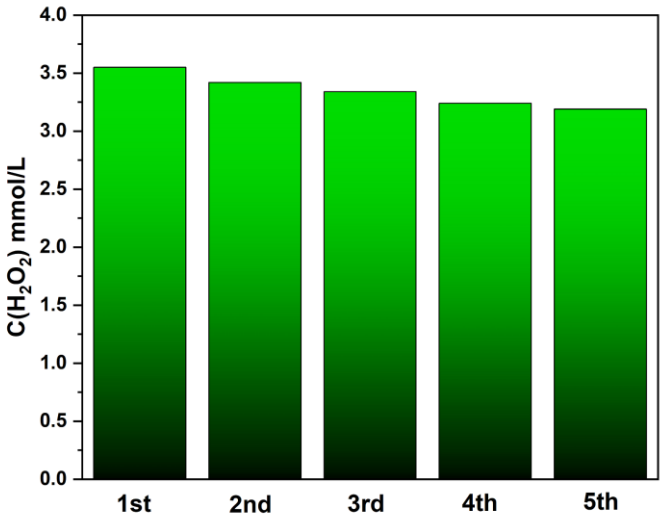

Figure S6. Long-term stability tests on the TiO_2(B)-1 system for H_2O_2 production in plasma.

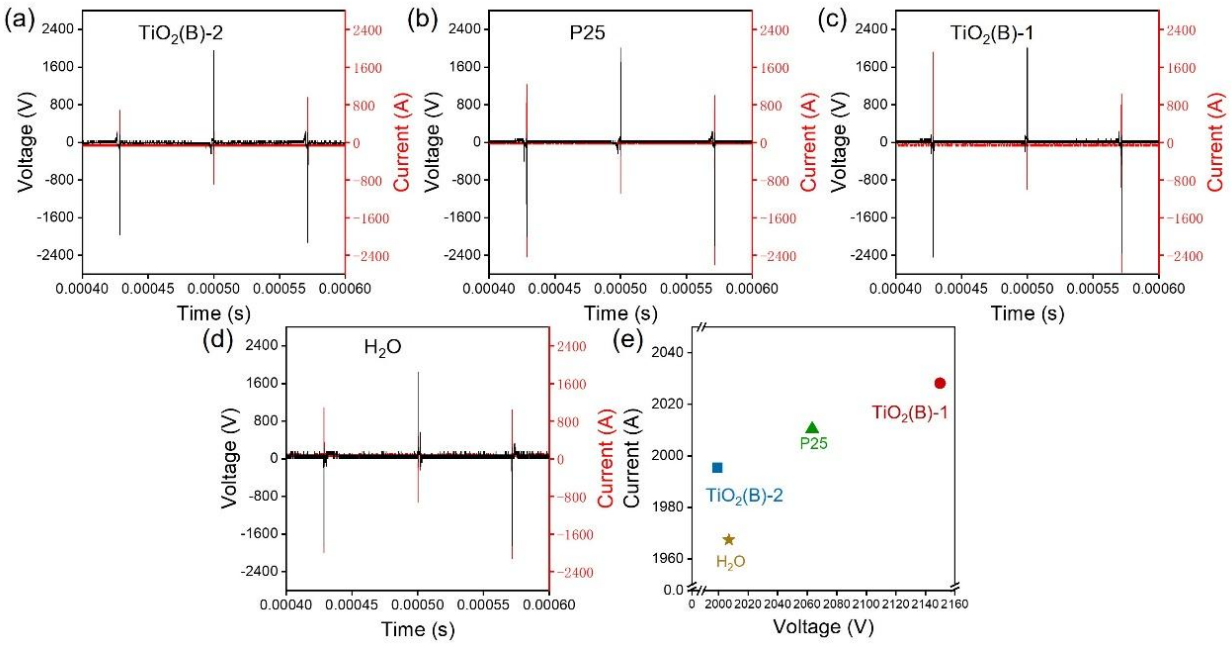

Figure S7. Voltage and current signals of plasma-catalysis system with different catalysts: (a) TiO_2(B)-2; (b) P25; (c) TiO_2(B)-1; (d) without catalyst. (e) Schematic illustration of the actual power with different plasma-catalysis systems.

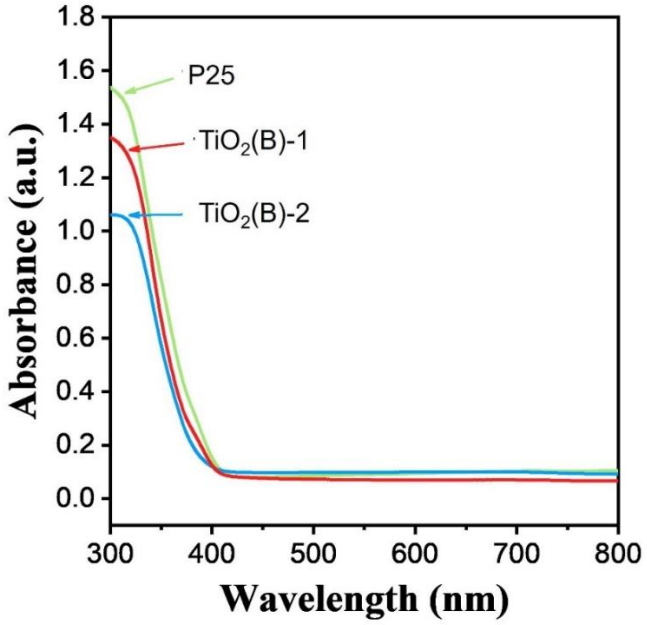

Figure S8. UV-Visible absorption spectra of different samples

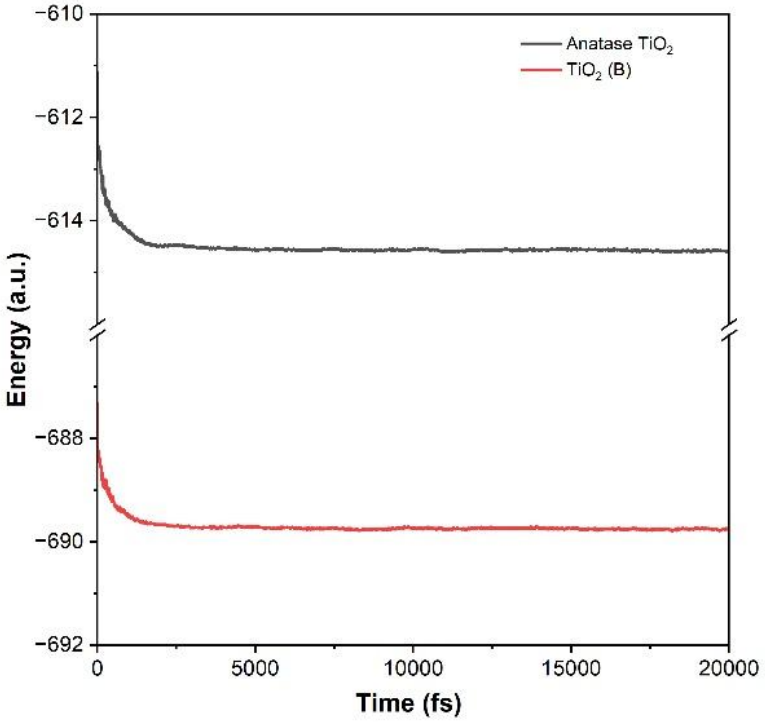

Figure S9. Kinetic energy variation curves of two systems over time.

Table S2: Plasma Emission Spectra Data (Normalized to Na Atom)

Material	Hα line intensity (656.7 nm)	O line intensity (777.5 nm)	O line intensity (845.2 nm)
H_2O	16.13	18.96	4.56
P25	18.96	30.67	6.43
TiO_2(B)-1	18.93	30.68	12.36
TiO_2(B)-2	16.16	25.48	5.61

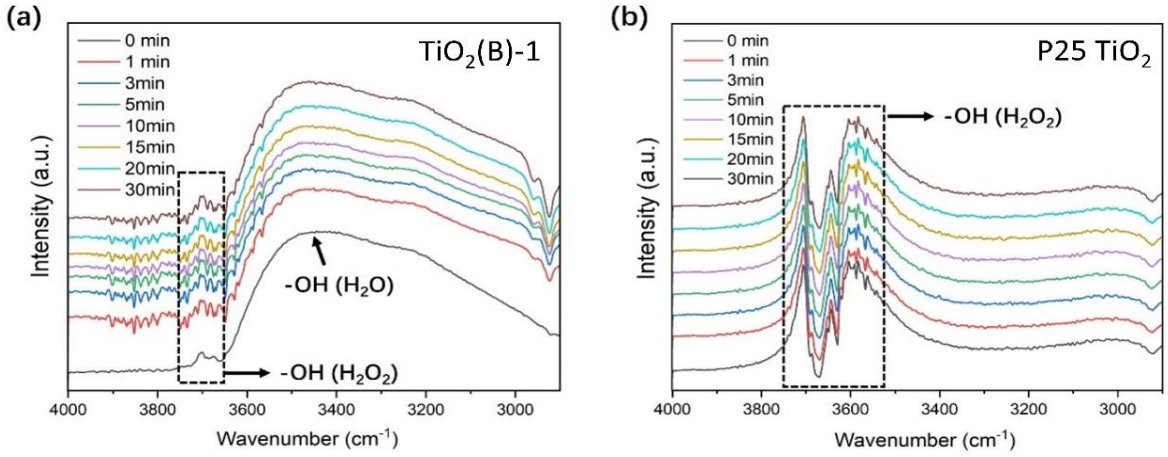

Figure S10. In-situ FT-IR of TiO_2 during the irradiation of H_2O_2/TiO_2 sample: (a) TiO_2(B)-1; (b) P25 TiO_2.

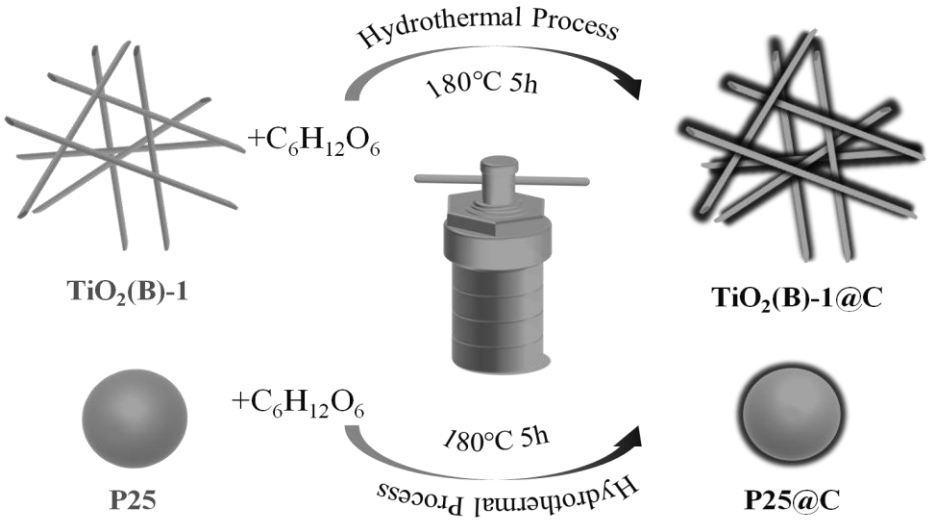

Figure S11. Scheme for coating carbon layer on TiO_2 samples.

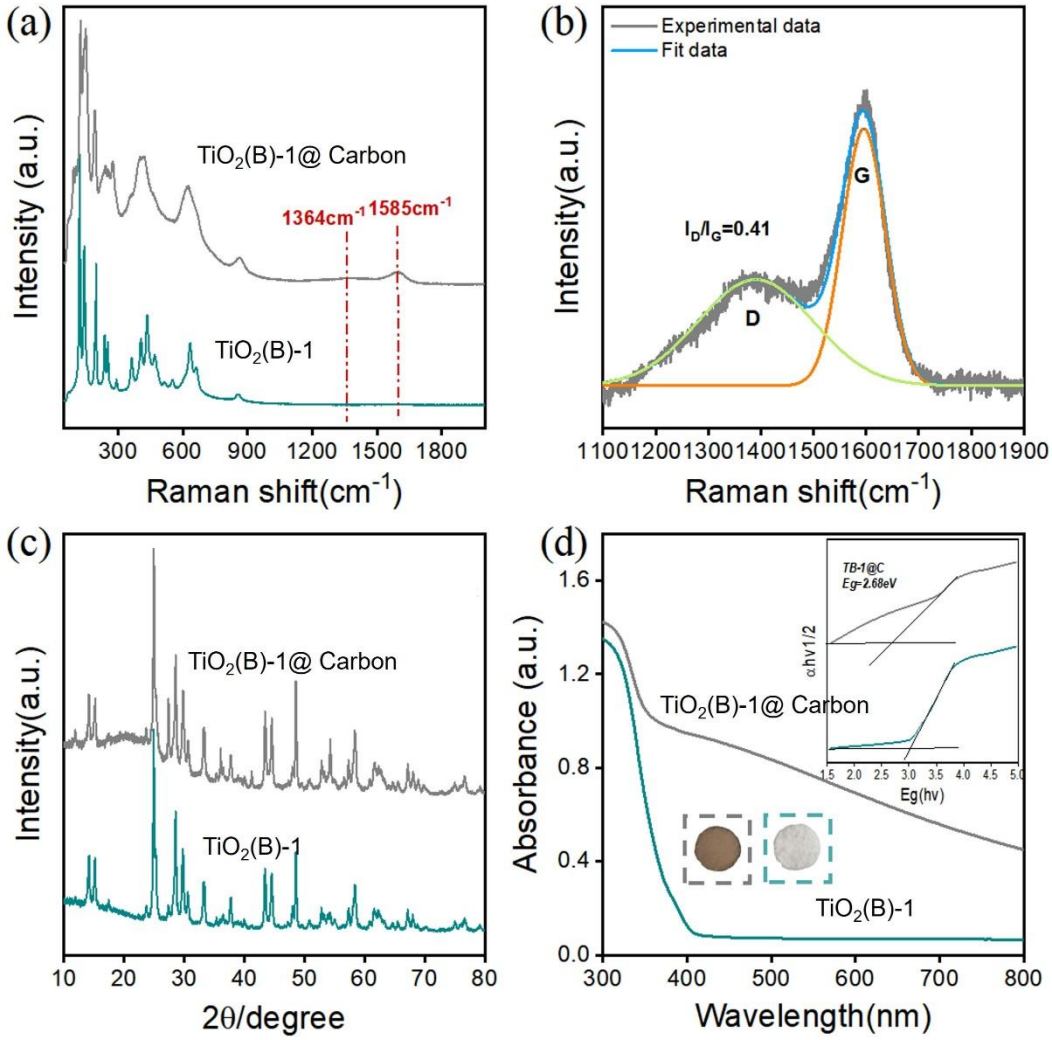

Figure S12. Structural characterization of TiO_2(B)@C catalyst: (a) Raman spectra, (b) Raman spectra of carbon peaks, (c) XRD patterns, (d) UV-Vis diffuse reflectance spectra.

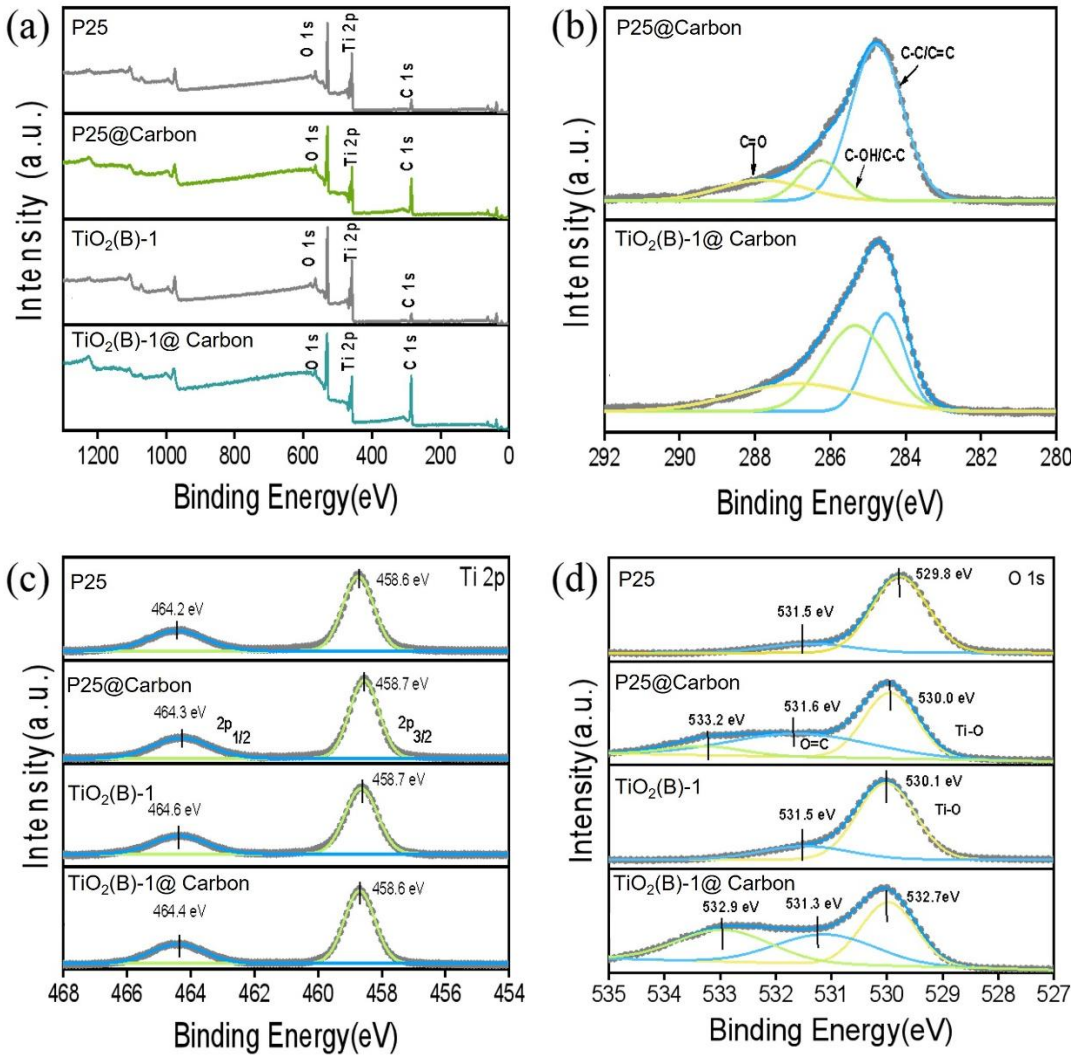

Figure S13. XPS survey spectra of different samples (a) and high-resolution XPS spectrum of the carbon element (b), titanium element (c) oxygen element (d) on the surface of carbon-loaded samples.

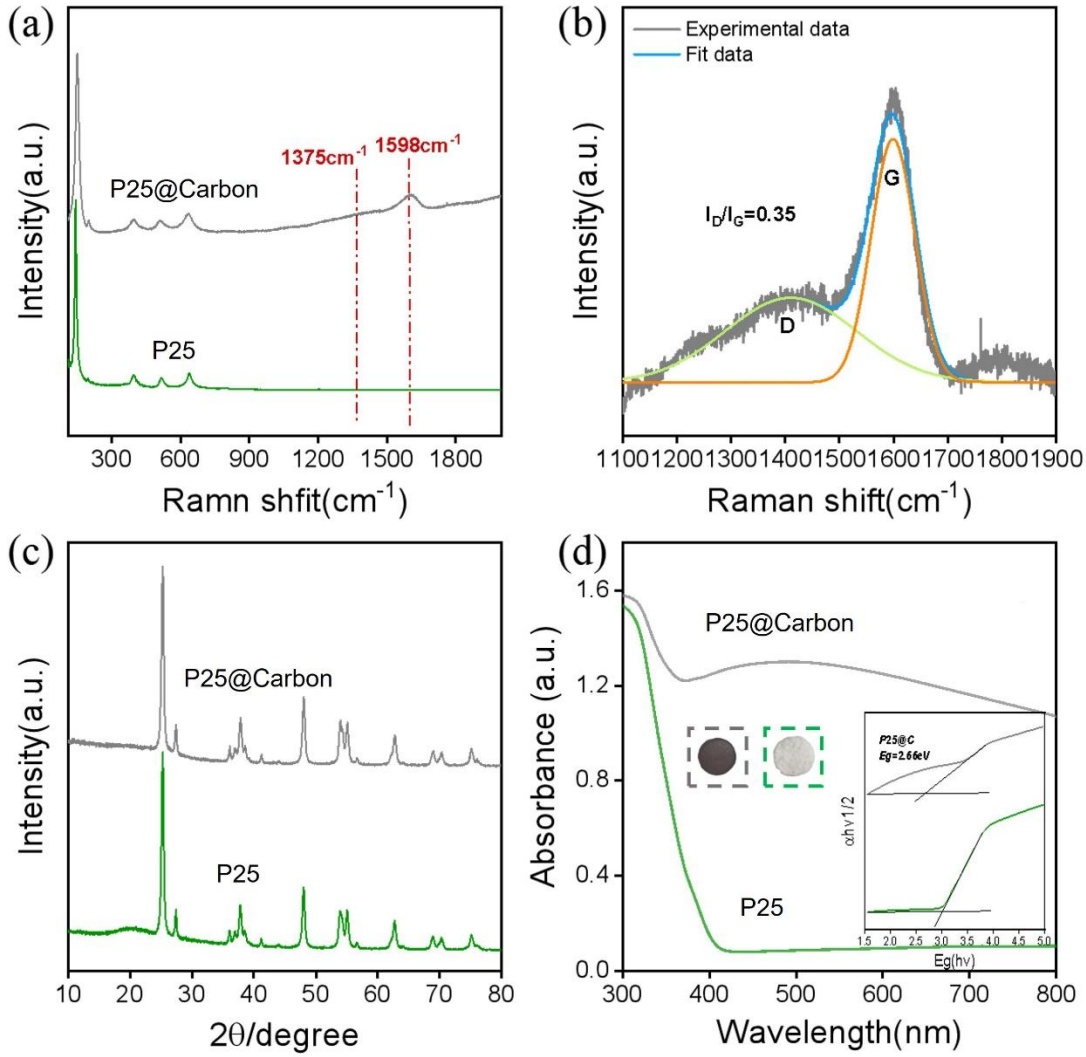

Figure S14. Structural characterization of P25@C catalyst: (a) Raman spectra, (b) Raman spectra of carbon peaks, (c) XRD patterns, (d) UV-Vis diffuse reflectance spectra.

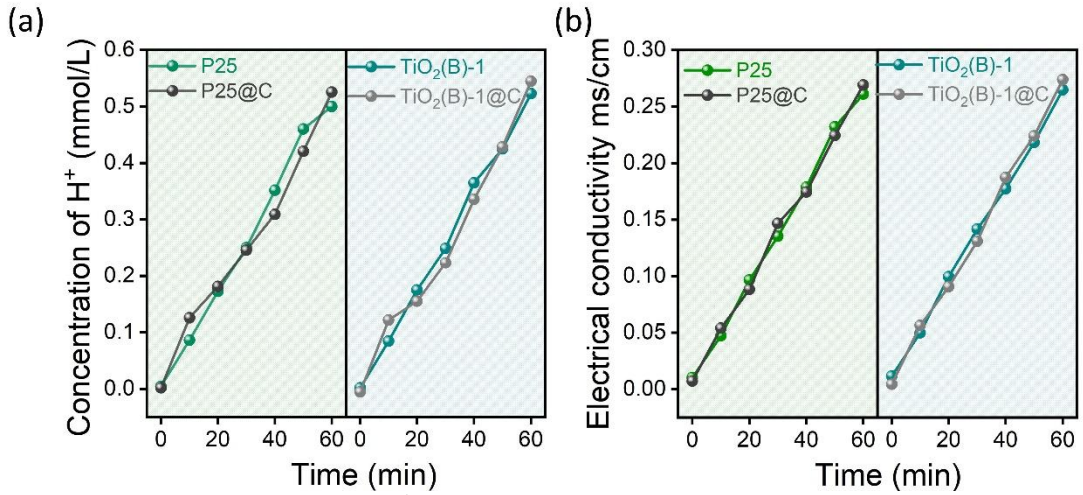

Figure S15. Concentration of H^+ and conductivity over different TiO_2 coupled plasma systems.